



A rechargeable lithium-ion battery module for underwater use

David R. Pendergast^{a,b,*}, Edward P. DeMauro^{a,c}, Michael Fletcher^a, Eric Stimson^a, Joseph C. Mollendorf^{a,c}

^a Center for Research and Education in Special Environments, University at Buffalo, Buffalo, NY 14214, United States

^b Department of Physiology and Biophysics, University at Buffalo, Buffalo, NY 14214, United States

^c Department of Mechanical and Aerospace Engineering, University at Buffalo, Buffalo, NY 14214, United States

ARTICLE INFO

Article history:

Received 6 April 2010

Received in revised form 21 June 2010

Accepted 22 June 2010

Available online 30 June 2010

Keywords:

Li-ion battery performance

DC battery power

Underwater

Pressure resistance

Thermal

ABSTRACT

Portable underwater electrical power is needed for many commercial, recreational and military applications. A battery system is currently not available to meet these needs, which was the aim of this project. Lithium-ion battery cells (Panasonic (CGR18650E)) were chosen, based on their high energy density and availability. To increase their voltage, 8 battery cells were connected in series (“sticks”) and protected by encapsulating them into a polycarbonate tube; and 6 sticks were housed inside a triangular aluminum case (module). Testing was performed to determine the consistency of individual cells, sticks and module and during discharge/charging cycles. The effect of ambient temperature (T_A) was determined by instrumenting them with thermocouples. In addition, voltage and current were measured and used to determine the heat generated within the battery cell and were compared to theory. From these data, a radial temperature profile was determined for two battery sticks in the battery module. Collapse pressure was determined and compared to theory. The Panasonic (CGR18650E) cells delivered 2291 mAh each over a wide range of T_A and discharge/charge rates. The theoretical and experimental data showed that the temperature within the battery sticks and modules did not rise above or below their operating temperature range (−20 and 60 °C), in agreement with the models. The tubes encapsulating the sticks withstood pressures down to 305 m of sea water (msw) which was predicted by modeling. The Panasonic (CGR18650E) cells, sticks and module demonstrated that they provided sufficient electrical power, reliably and safely to be used in the underwater environment (1800–2000 kPa, 305 msw) over a wide range T_A , including high power requirement systems like an active thermal protection system that keeps a diver comfortable in extreme temperature conditions. The concept developed here can be modified to meet specific power requirements by varying the number of cell in series to achieve the desired voltage, and the number of sticks in parallel to provide the current capacity required.

© 2010 Elsevier B.V. All rights reserved.

1. Introduction

Underwater activities are widespread in commercial, sport and military groups. All of these groups use devices and equipment to require electrical power of varying magnitudes, and for portability battery power is ideal. In addition to lighting and power tools, a new technology that maintains the divers’ thermal balance increases the need for a more rigorous battery power system [1]. Ideally this battery system would operate in waters ranging from −2.2 to 40.5 °C down to a depth of 107 m of sea water (msw) for an indefinite time [2]. Other requirements included that it be rugged, not decrease mobility, be neutrally buoyant, be waterproof, have a low drag

coefficient, be resistant to punctures and abrasion, have redundant components, highly reliable and cost effective [2].

Previously, it has been reported that battery packs for thermal extremes that included Li-Ion batteries, a control board, temperature sensors and an enclosure are possible [3]. Lithium-ion battery cells have a high energy and power density, when compared to other reusable battery cells, such as silver/zinc battery cells [4] and they are rechargeable. Lithium-ion battery cells are designed with safety vents in the case of a sudden increase in cell pressure [5]. In the event that pressure increases, a membrane on the top of the battery is punctured to allow for pressure venting [5]. Likewise, to avoid the possibility of a thermal runaway, there are PTCs which function as thermal fuses built into the battery to stop use, and are generally set to blow around 30–50 °C above the upper temperature limit [5]. In addition, the battery must not be exposed to water, since this could cause a short circuit. If a prolonged short circuit was to occur, this could cause the battery to heat up and ignite the contents [6,7].

* Corresponding author at: Center for Research and Education in Special Environments, University at Buffalo, 124 Sherman Hall, 3435 Main Street, Buffalo, NY 14214, United States. Tel.: +1 716 829 3830; fax: +1 716 829 2384.

E-mail address: dpenderg@buffalo.edu (D.R. Pendergast).

Nomenclature

a	distance between the center points of two cylinders (m)
A	area (m^2)
α	thermal diffusivity ($\text{m}^2 \text{s}^{-1}$)
Bi	Biot number
b	radius (m)
β	volumetric thermal expansion coefficient (1 K^{-1})
β_m	eigenvalue
c	specific heat ($\text{J kg}^{-1} \text{K}^{-1}$)
Δr	stepsize (m)
Δt	timestep (s)
g	gravity (m s^{-2})
$h_{\text{Cond.}}$	conduction heat transfer coefficient ($\text{W m}^{-2} \text{K}^{-1}$)
$h_{\text{Conv.}}$	convection heat transfer coefficient ($\text{W m}^{-2} \text{K}^{-1}$)
$h_{\text{Rad.}}$	radiation heat transfer coefficient ($\text{W m}^{-2} \text{K}^{-1}$)
H	height (m)
I	current (A)
k	thermal conductivity ($\text{W m}^{-1} \text{K}^{-1}$)
N	Number of cylinders
Nu	Nusselt number
φ	angular coordinate (rad.)
Pr	Prandtl number
\dot{Q}	heat generation (W)
\dot{q}	volumetric heat generation (W m^{-3})
ρ	density (kg m^{-3})
Ra	Rayleigh number
R	radial dummy variable (m)
r	radial coordinate (m)
S	shape factor (m)
T	temperature (K)
T_∞	air temperature (K)
θ	temperature difference (K)
t	time (s)
τ	time dummy variable (s)
u	homogenized temperature difference (K)
V	volume (m^3)
V	operating voltage (V)
V_{OC}	open-circuit voltage (V)
z	axial coordinate (m)
D	outer diameter of the tube (m)
d	mean diameter of the tube (m)
E	Young's modulus of elasticity (N m^{-2})
L	length of the tube (m)
L_c	critical length (m)
ν	Poisson's ratio
P_c	collapse pressure (N m^{-2})
t	thickness of the tube (m)
yc	compressive yield strength (N m^{-2})

Based on their design characteristics, lithium-ion batteries offer great potential for underwater use, however, there are a large number of design challenges to make them functional and safe in water, under high pressure, and in extreme temperatures. Thus, the purpose of this project was to design and test a rechargeable lithium-ion battery module for underwater use. Analytical, numerical, and experimental methods were used to: (1) select the appropriate lithium-ion battery from available choices, (2) design a battery stick capable of providing enough power by combining single lithium-ion battery cells in series, (3) combine these sticks in parallel for increased capacity, (4) evaluate the effects of external temperature and pressure on performance of individual lithium-ion and combinations of cells, (5) evaluate the overall tem-

perature distribution resulting from the cells exothermic reaction, and finally, and (6) develop a pressure resistant container for the battery sticks.

2. Methods

2.1. Battery cells

2.1.1. Individual battery cell selection and testing

The first step in this process was to evaluate potential battery cell availability. Cells from A123 Batteries America (2LP1900, 2LP405590P4H), Common Sense (LP-2S2000-8-X2), Dualsky (XP22502), Enerland (PF415585), Kokam, Lucky Goldstar (LG) (E1, E2, LG18650-2400-T4), Panasonic (Lilon, CG18650E), Saehan Enertech (SPB496395, 366395, 605060), Sanyo (UPF574199), TENERGY (PL-00550100, 7552146, 7458168, and Li8650-2200-4), Thunderpower (TP2100-2S), Tronics Huizhou, and Ultralife SSS were evaluated for their voltage, capacity, discharge amperage capacity, shape and size, cost and availability. Based on this analysis three Li-Ion batteries were selected for further evaluation and compared to a Li-polymer batteries that were previously used in testing in our laboratory. From this analysis, two Li-ion batteries were selected for testing; i.e. LG (LG18650-2400-T4) and Panasonic (CGR8650E) as they had the greatest capacity (2400 and 2550 mAh, respectively), volumetric capacity (0.145 and $0.154 \text{ mAh mm}^{-3}$, respectively) and specific capacity (per unit battery weight, mAh gm^{-1}) and were widely available and used.

The LG and Panasonic battery cells were tested for consistency among cells ($n = 5$) and duty cycles (5 cells cycled 5 times) by recording discharge capacity as a function of time. From this measure, their capacity was determined (mAh) and compared among batteries and conditions. These batteries were also tested for the effect of discharge and charge rates on capacity, as well as compared to the manufacturers' specifications. The effects of discharge rates and ambient temperature (0 – 55°C) on capacity were determined as well. The batteries were discharged and then charged (Intelli-Peak ICE Charger) and the data recorded on a computerized data collection system (DAQ, IOTech).

Battery Specialties (Costa Mesa, CA) was identified, and with approval of Panasonic, Inc., eight (8) cells were arranged end-to-end geometrically and in series electrically to form a stick. Each stick had incorporated a charging/discharging and electrical protection circuitry board to provide nominally 28.8 V per stick. This protection circuitry prevented over-voltage (4.2 V max), under-voltage (3 V min), over-current discharge (30 A max), over-current charge (10 A), over-temperature (55 – 60°C), short-circuit protection, constant current/constant voltage (CC CV^{-1}) charging, and cell balancing for each individual cell. The circuit consumes only $20 \mu\text{A}$ on discharge and $140 \mu\text{A}$ during charging, effectively eliminating the impact of the controller on discharge capacity. The stick was then enclosed in a polycarbonate tube, with a length of 0.54 m and a wall thickness of 1.60 mm .

The next step was to combine the battery sticks electrically in parallel into a battery module. An equilateral triangular shape was selected as a compact modular arrangement for this application, and designed for 6 sticks per triangle (48 battery cells, 14.88 kg mass, and 75.9 cm in length and 12 cm sides). With the standard capacity of 2000 mAh , combining battery sticks in parallel increase the capacity of the system, with the amount determined by the number of sticks arranged in parallel.

2.1.2. Battery stick thermal analysis

Due to the electrochemical reaction inside the battery cell, heat is generated as the battery is either charged or discharged, affecting the temperature distribution within the battery cell. Temperature

is an important consideration with Li-ion batteries, since they must remain within a fixed range during discharge (-20 – 60 °C) and charging (0 – 45 °C) [8,9]. If this temperature range is exceeded, the battery cells may ignite due to “thermal runaway” [5]. Although the use of a thermal sensor has been suggested in battery pack design [3] this adds considerable complexity to the pack. Many previous investigators have developed thermal models of lithium–polymer batteries [10–13]. The method used in this study employed the heat conduction equation, in cylindrical coordinates [14,15]:

$$\frac{1}{\alpha} \frac{\partial T}{\partial t} = \frac{1}{r} \frac{\partial}{\partial r} \left(r \frac{\partial T}{\partial r} \right) + \frac{\dot{q}(r, t)}{k} z \quad (1)$$

Here, it is assumed that all thermal properties are constant and that temperature variation is negligible in the axial (z) and azimuthal (φ) directions. It was also assumed that the conductivity and other heat transfer/thermodynamic properties of the batteries could be represented by an average value across the various components of the battery. The justification for this was taken from previous work [20], that showed it was possible to derive a composite values for these properties, and it was assumed that the batteries used in the present study would not differ to largely from these values, and therefore their values were used in the evaluation of the temperature distribution of the batteries. The equation describing the heat generation is given by [10–13]:

$$\dot{Q} = I \left(V_{oc} - V - T \frac{\partial V_{oc}}{\partial T} \right) \quad (2)$$

In Eq. (2), I is the load current, and V_{oc} and V are the open-circuit and load voltage, respectively. According to Pals and Newman [10], the last term on the right-hand side of Eq. (2) describes the reversible entropy change in the battery cell. Chen and Evans [16] state that when discharging at a high rate, the heat generation curve is mainly determined by the difference in the open-circuit voltage and the operating voltage.

The geometry and coordinates of a single battery cell that was used in the mathematical model is used in Eq. (1) which also requires that both an initial condition and two boundary conditions be specified. The initial condition and the boundary condition at the surface are determined from experimental data. At the center of the battery cell, symmetry is invoked, meaning that the boundary condition at $r=0$ is treated as if it were adiabatic, and the solution must be finite at this location, $dT/dr=0$. Likewise, because Eq. (1) is second order in space, it will have two linearly independent solutions, as mentioned by Haberman [17]. One solution must be eliminated since it will go to infinity at $r=0$.

It is noted that the boundary conditions and Eq. (1) are non-homogeneous and that an analytic solution cannot be found using separation of variables, as mentioned by Haberman [17]. Özişik [18] gives an analytic solution for Eq. (1), using a Green’s function. As a check, a numerical solution was performed using methods given by Hoffmann and Chiang [19].

The numerical solution of Eq. (1) can be carried out explicitly using a finite difference method [15,19]. A forward time/central space explicit method was incorporated using a Taylor series expansion, where the central differences for the temperature derivatives are given by Hoffmann and Chiang [19].

Both the analytic and numerical solutions were used for finding the heat flux through the surface of the battery. The average composite properties of the battery cells needed for both the analytical and numerical solutions are taken from Maleki et al. [20]. As these values are generally functions of temperature, Chen and Evans [16] state that it can be assumed that the constants represent average values over the range of temperatures that were analyzed in this study.

2.1.3. Battery temperature numerical solutions

A code was written to solve Eq. (1) using an explicit finite difference approach. The polynomial expressions for the surface temperatures and heat generation sources were coded into the program. A Fourier number of 0.4 was chosen, along with a timestep of 0.025 s. Mathematica was used to solve for the temperature as a function of time, and also for the transfer coefficients. For battery stick 1 (Fig. 5) L was taken to be the distance from the corner of the aluminum battery module to center of the battery, minus the radius of the battery to be 12.7 mm. For battery stick 2 etc. the distance between battery stick centers and their distance from the container wall, as well as the battery stick diameter were used. The heat generation, area, and volume were divided by two to account for the pocket of air between the two battery sticks.

2.1.4. Battery stick pressure resistant testing

The behavior of cylindrical shells exposed to external pressure has been well explored [21]. Many relationships to describe the behavior of long tubes, with lengths greater than their critical lengths, exposed to external pressure [21–23], as well as in short thin tubes [24] and this was revised for thickness ratios as low as 10 [25,26]. In addition, equations for the calculation of collapse pressure, depending on tube length and thickness have been reported [25,26]. More recent work considers how tubes may react under additional types of loading, such as combined internal and axial loading and interactions thereof, while considering the contributions from the end-conditions [27].

The tubes used for this investigation have LD^{-1} and Ld^{-1} ratios of about 21 and 23, respectively. The minimum length for each tube beyond which the collapsing pressure is constant (critical length) to be used to determine the appropriate formula for the collapsing pressure is given by the equation [28,29]:

$$L_c = 1.73 \sqrt{\frac{d^3}{t}} \quad (3)$$

Using Eq. (3), the critical length of the tubes used in this investigation was about 152 mm. Because this value is less than the length of the tube (long tube) the end-effects of the tube can be ignored [28]. The Dt^{-1} and dt^{-1} ratios for the tubes in this investigation are small enough to be considered thick, 16 and 15, respectively, and thus the collapse pressure for thick tubes which is determined by inelastic behavior was used [26].

Previous studies have provided the background [21,24,30] for the method used in the present study for estimating the collapse pressure of tubes made of two different materials, specifically: acrylic and polycarbonate.

2.1.5. Measurement of collapse pressure

An experiment was performed to evaluate the collapse pressure of tubes made from acrylic and polycarbonate and the data were compared to that calculated from published models [22,25]. A cast iron water tank (71 cm in diameter with 2.54 cm wall rated to 1701 atmospheres) was used to pressurize the tubes via an air pump and water supply. A pressure gauge was connected to the air pump to measure the pressure of the air pumped into the water tank. The water used was boiled to remove any dissolved gases and then allowed to cool to room temperature. An acrylic or polycarbonate tube was filled completely with the boiled water and a fitting with Swagelok tubing screwed into its top. The two-sided fitting was screwed into the tube and to the top of the water tank.

The tank was filled with water at a specified temperature until it was completely full; room temperature water for the acrylic tube tests and temperatures of 11.7, 13.4, 21, 40.8, and 42.1 °C for the polycarbonate tube tests. A graduated pipette was attached to the top of the fitting. Air was pumped into the tank, and the

pressure was increased incrementally. Water was squeezed out of the tube as the tube deformed, into the graduated cylinder. The volume of the ejected water was recorded as a function of the tank pressure. The tank pressure was increased until the tube failure.

2.1.6. Polycarbonate tube vise test

This experiment was done to determine how the volume of the tube was affected by collapse due to external pressure. A polycarbonate tube was filled with water, as described above, and a fitting was attached to the top of the tube and the graduated pipette. The tube was placed inside of a vise between pieces of plywood used to distribute the force of the vise along its axial length. A caliper was used to measure the minor diameter of the elliptical cross-section of the tube as a function of volume deformation as water was ejected into the graduated pipette. Compression with the vise continued until the minor diameter of the tube ceased to change noticeably, which was taken to be the smallest diameter of the tube. Once the smallest diameter was reached, the vise was opened slowly, using the same method, in order to explore how well the tube recovered from compression.

2.1.7. Polycarbonate reliability test

An experiment was conducted to study prolonged pressurization on polycarbonate tube performance. The experimental apparatus was comprised of a stainless steel tube connected to a nitrogen tank and a water tank. A polycarbonate tube was prepared, as described above, with the fitting screwed into the stainless steel tube. The whole assembly (N_2 tank and stainless steel tube) was filled completely with water ranging between 10 and 40 °C, and a coaxial knob was closed to seal the tube. Nitrogen was supplied to increase the pressure inside the stainless steel tube on the polycarbonate tube, which forced water out through an exhaust. The assembly was pressurized to 1034 kPa (simulating 107 m water depth). The pressure was held for 2 h, after which the pressure was suddenly released by turning off the nitrogen gas supply and venting the system through the coaxial exhaust. The polycarbonate tube was removed, and the remaining volume was re-measured.

3. Results

3.1. Battery selection

Selected battery cells were rejected from further consideration due their rectangular shape and low capacity or capacity per unit volume or weight (Batteries America, Common Sense, Dualsky, Enerland, Kokam, Saehan Eneritech, Sanyo, TENERGY, Thunderpower, Tronics Huizhou, and Ultralife SSS). The capacity levels were about 50% of that of the selected batteries. One battery was very expensive and fragile (Thunderpower).

LG batteries were compared to Panasonic Li-ion batteries based on the rate of discharge as a function of time, consistency of power supplied by individual batteries, and the consistency of power during charge/discharge cycles. Both the LG and Panasonic batteries discharge and charge capacities among batteries were consistent during discharge with coefficients of variation (s.d. divided by mean) of 1.5–3%. Similarly, the capacities during repeated cycling were very consistent among the cycles, with coefficients of variation of 1.5–2.0%. The major difference between the LG compared to Panasonic Li-ion batteries was the rate their capacity decreased and the capacity where they failed. In the latter case the range for LG was 2000–2500 mAh (data not shown) and for Panasonic Li-ion 2250–2500 mAh for discharge rates \sim 2500 mA (see Fig. 1). Based on these test results and the common availability and use, the Panasonic cells were selected for further testing.

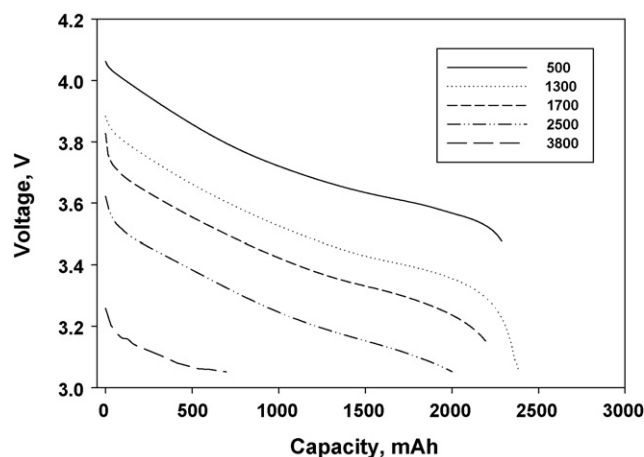


Fig. 1. Voltage is plotted as a function of capacity for the average of 5 individual cells during discharge at rates of 500–3800 mAh.

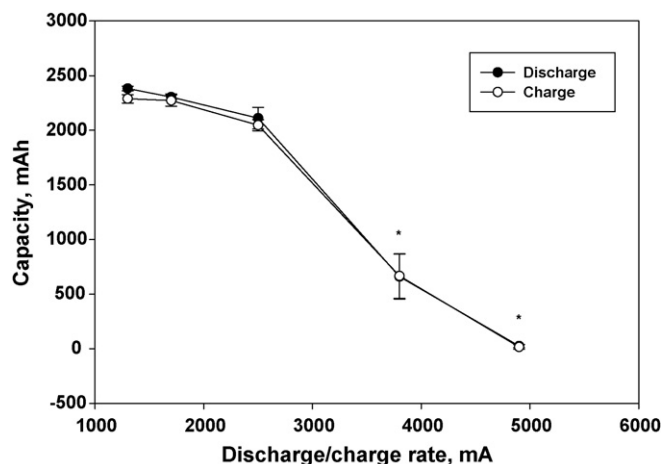


Fig. 2. Average values (\pm s.d.) for capacity are plotted as a function of discharge and charge rates for 5 cells tested individually. The * indicates the values are significantly different from the 500 mA value at the $p=0.05$ level.

The individual battery cells have a diameter of 18.5 mm and a length of 65 mm. The mass of one battery cell is 43 g. Each battery cell has a standard capacity of 2000 mAh, with a nominal voltage of 3.6 V [31]. The operating temperature range for the battery cells is between -20 and 60 °C during discharge and 0 and 45 °C during charge [9]. Relevant thermal properties for the battery cells include a composite conductivity value of 3.4 W m K^{-1} , and composite diffusivity value of $1 \text{ e-}6 \text{ m}^2 \text{ s}^{-1}$ [20]. Over a discharge/charge rate of 500–2500 mA there was no significant effect on capacity which averaged $2265 \pm 139 \text{ mAh}$ (Fig. 2), however it was significantly decreased at 3800 and 5000 mA discharge. Similarly the batteries' capacity was not significantly affected by temperature from an ambient temperature of $55\text{--}25$ °C ($2316 \pm 116 \text{ mAh}$), while it was lower at 15 and 0 °C (34%) (Fig. 3).

Based on the analysis described above, the Panasonic battery cells were selected to make the battery sticks (see Fig. 5), which were subsequently tested using the same protocols used for the individual cells. Sample data are shown for the discharge of a battery stick, and its comparison to Panasonic's specifications, in Fig. 4. As can be seen the data for the stick discharged at 1700 mA is similar to that of individual cells (Fig. 1) and in agreement with the manufacturer's specifications [9,31]. The stick also passed the other tests of discharge rate and temperature (data not shown), and thus were incorporated into a battery module (Fig. 5).

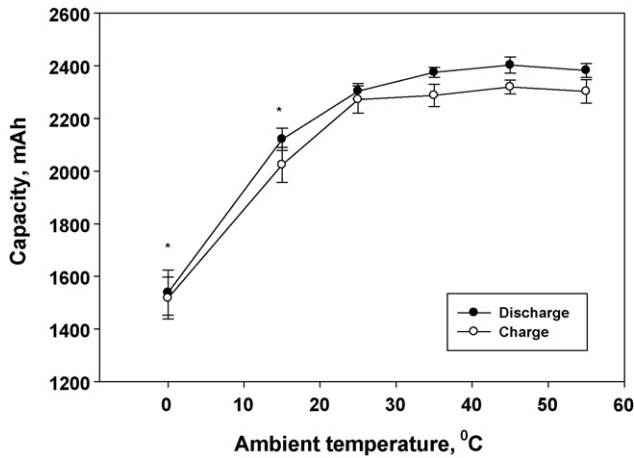


Fig. 3. Average values (\pm s.d.) for capacity are plotted as a function of ambient temperature for 5 cells tested individually for charge and discharge at 1700 mAh. The differences between charge and discharge were not significantly different from each other. The * indicates the values are significantly different from the 55 °C value at the $p=0.05$ level.

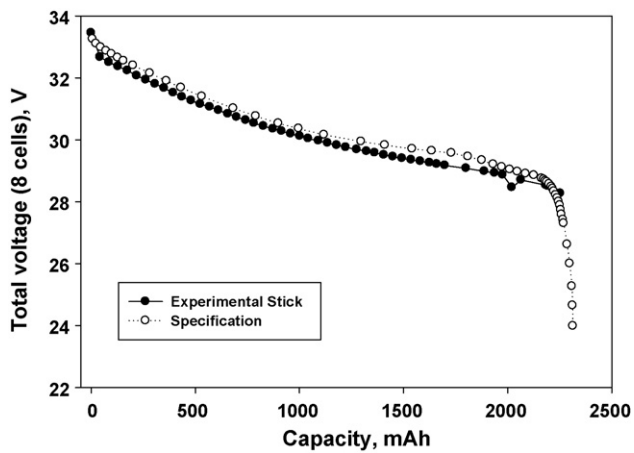


Fig. 4. Total voltage from 8 cells in series is plotted as a function of capacity during discharge and compared to the specifications given by Panasonic for the CGR8650E batteries.

3.2. Thermal experimental data for battery sticks

Experimental data showing the open-circuit voltage changes in a battery stick as a function of temperature are shown in Fig. 6. The slopes of the lines in Fig. 6 are $-1.11\text{E-}04\text{ V K}^{-1}$ when increasing temperature, and $-9.34\text{E-}05\text{ V K}^{-1}$ when decreasing temperature.



Fig. 5. The battery stick comprised of 8 individual Panasonic cells is shown along with the circuit board used for charging and discharging and safety. A meter stick is shown for reference.

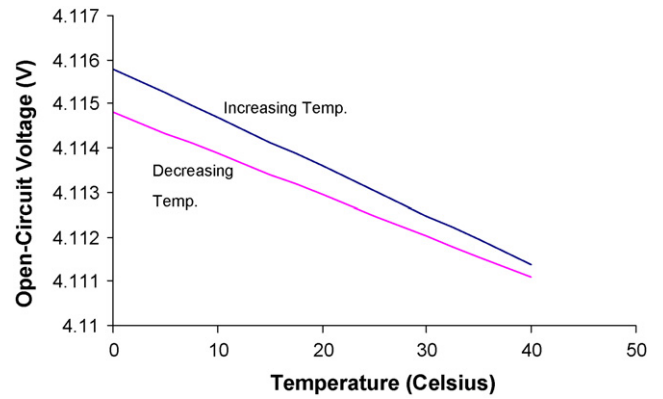


Fig. 6. Open-circuit voltage is plotted as a function of increasing and decreasing temperature for a battery stick.

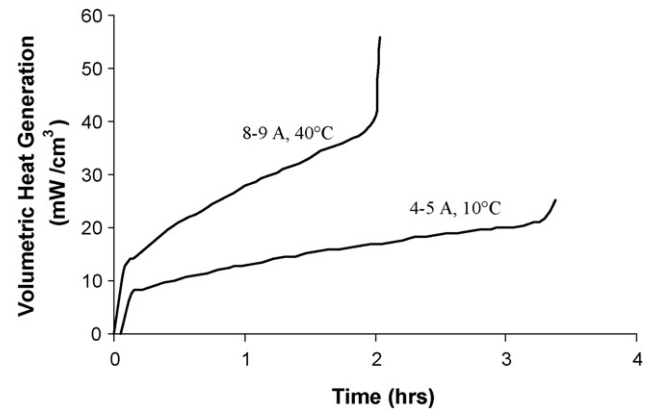


Fig. 7. Volumetric heat generation corresponding to two different temperatures, using Eq. (1) is plotted as a function of time.

This hysteresis is likely due to a slight voltage drain in the battery cells during the experiment.

The heat generation was calculated from the voltage and current data using Eq. (2). The current, between 8 and 9 A or 4 and 5 A, was divided by six, in order to estimate the average stick current; likewise the voltage difference was divided by eight to estimate the average voltage per cell. Fig. 7 shows the resulting heat generation for 10 and 40 °C water. A non-linear regression was performed in Mathematica, fitting the data to a 6th degree polynomial. The resulting polynomials were used in both the analytical and numerical solution methods. For the 10 °C water case, the R^2 value was 0.998; for the 40 °C water case, the R^2 value was 0.996. Measured surface temperatures for sticks 1 and 2 in 10 °C water stated at 18 and 21 °C and decreased exponentially to a steady state of nominally 13 and 15 °C, respectively, after 1 h. Measured surface temperatures for sticks 1 and 2 in 40 °C water stated at 31 and 26 °C and increased exponentially to nominally to 46 °C after 3 h.

Surface temperatures were fit with the 6th order polynomials (Mathematica) that were then used in the model solutions. In 10 °C water, the surface temperatures for sticks 1 and 2 had R^2 values of 0.99 and 0.99, respectively. Likewise, sticks 1 and 2 had R^2 values of 0.99 and 0.99, respectively for 40 °C water. The surface temperatures correspond to the boundary condition, $T(b, t) = f(t)$.

3.2.1. Analytical and numerical solutions for battery temperature measurements

An example of the radial temperature distributions at various temperatures comparing the numerical and analytical solutions for stick 1 at 10 °C are shown in Fig. 8. The purpose of this analysis

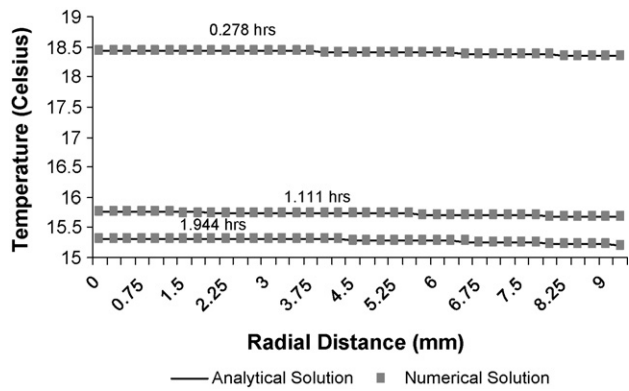


Fig. 8. Radial temperature distribution in stick 1 in 10 °C water. Solid lines indicate the analytical solution, while filled squares are the numerical solution.

was to test if the battery stick under these operating conditions remained within its safe operating conditions. Similar analysis was performed for stick 1 and 40 °C and for stick 2 under both conditions. It can be seen in Fig. 8 that the temperature distribution is relatively constant across the radius, which was also the case for stick 2 and in 40 °C. For the cold water cases, the radial temperatures decrease as a function of time ($1.57\text{ }^{\circ}\text{C h}^{-1}$) and for the hot water case they increase with time ($8\text{ }^{\circ}\text{C h}^{-1}$); and there was no significant difference between the two sticks ($p = 0.469$) or the Analytical and Numerical Models ($p \geq 1.00$). Percentage differences in the model solutions were calculated to be less than 0.03%. The numerical solution contains truncation errors due to the application of Taylor series, where there are two central differences for the radial coordinate, and have an accuracy of order $(\Delta r)^2$, while the forward difference for the time derivative has an accuracy of order (Δt) . Oscillations in the errors graphs are dependent on the number of terms used to calculate the analytical solution. The more terms (18 or more) used in calculating the analytical solution, the frequency of the oscillation increases, while their amplitude decreases; and resulted in a more accurate solution.

The centerline temperatures for the battery sticks were estimated using Eq. (1). Fig. 9 shows a comparison of the centerline temperatures along with the operating temperature range. The purpose of this analysis was to test if the battery stick under these operating conditions remained within its safe operating conditions. The profiles shown in Fig. 9 can be seen to remain within the thermal limits of the Li-ion battery cells. As can be seen from Fig. 9, the battery cells in this experiment are not in danger of violating the operating temperature limits. The temperature solutions also demonstrated that assuming the modes of heat transfer were

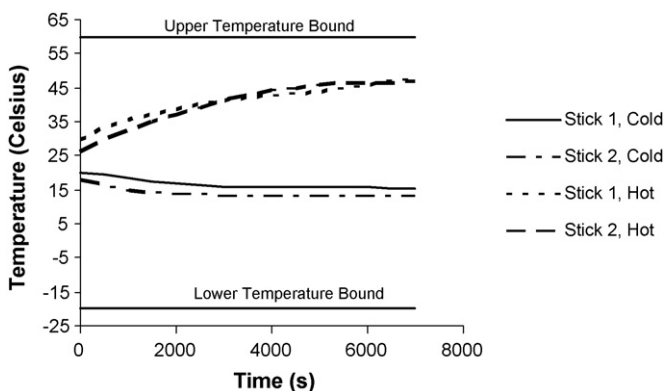


Fig. 9. Centerline temperatures for battery cells are plotted as a function of time for battery sticks 1 and 2 in 10 and 40 °C. The operating range provided by the manufacturer is also shown.

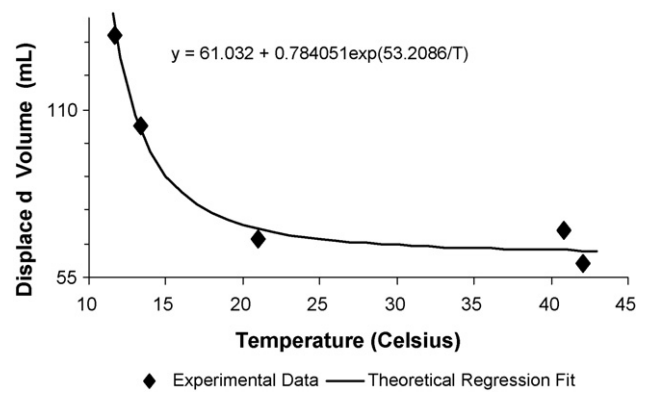


Fig. 10. The volume of water displaced from the tube during compression is plotted as a function of ambient water temperature.

conduction and radiation fit the experimental data better than the models assuming convection.

The radial temperature versus time data were used to calculate the heat flux across the surface of the battery cells. The battery sticks in hot water, initially had negative values for the heat flux, showing that heat is entering the battery sticks from the ambient environment (data not shown). This phenomenon raises concern when considering that the battery cells have a fixed operating temperature limit, as given by the manufacturer [9,31]. For this reason, the battery sticks must never be allowed to sit idle in a warm environment prior to usage, in order to ensure that the cell temperature does not rise above the upper temperature bound.

3.2.2. Collapse pressure test results

Acrylic tubes were tested and excluded from further consideration as while they crushed at a pressure twice that of polycarbonate ($2930 \pm 170\text{ kPa}$), as predicted by the various theories, they failed in a catastrophic manner, resulted in shattering; which would be detrimental in underwater applications. Fig. 10 shows the relationship between ambient water temperature and the volume of displaced water during compression. On average the tubes tested at 11.7–21 °C failed at $2068 \pm 170\text{ kPa}$, while between 40.8 and 42.1 °C they collapsed at 1896 ± 170 and $1724 \pm 170\text{ kPa}$, respectively. The trend line had an R^2 value of 0.99, implying that there is a functional relationship between the temperature and the displaced volume.

Data calculated from Southwell's [25] theoretical model was compared to experimental data, demonstrating that the collapse pressure was 27–39% less than the experimental value ($0.022 \pm 0.002\text{ Pcy}^{-1}$ compared to 0.015 Pcy^{-1} , non-dimensional values found through experimentation). The theoretical value predicted by Levy's [22] model more closely approximate the values obtained from testing, with differences are between 2 and 18% (0.016 Pcy^{-1} vs. $0.023 \pm 0.013\text{ Ccy}^{-1}$).

3.2.3. Polycarbonate vise test

The results of the Polycarbonate tube compression are shown in Fig. 11. The diameter was initially at 2.54 cm, and was compressed to 0.632 cm. It can be seen from Fig. 11 that as the tube is released, there is a slight hysteresis in the curve. The release curve, however, does not return to 2.54 cm, because permanent deformation occurred.

3.2.4. Polycarbonate reliability test

Polycarbonate tubes were pressurized to 1034 kPa eight (8) times in ambient water temperatures of 40 and 10 °C each. The volume of the tube after compressions in both temperatures was not different from the initial volume calculated from its geometry

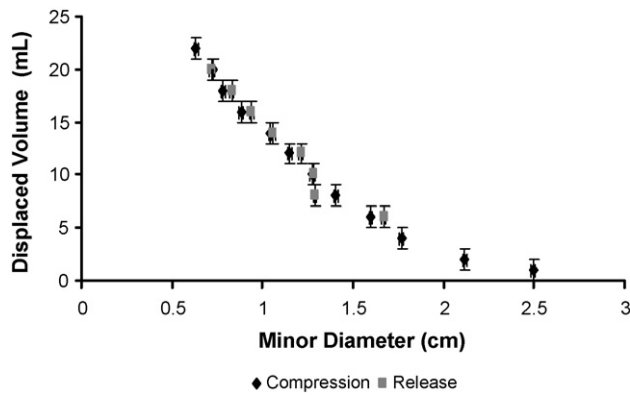


Fig. 11. The average (\pm s.d.) volume change in the polycarbonate tube while undergoing compression by a vise is plotted as a function of tube minor diameter of the tube.

(210 mL) (data not shown). Thus, the change in diameter of the tube at 1034 kPa is negligible.

4. Discussion/conclusions

4.1. Battery cell selection

The Panasonic (CGR18650E) battery was experimentally determined to have uniform capacity among cells and during cycling; and met the manufacturer's specifications [9,30] of capacity for discharge/charge rates of between 1300 and 2500 mAh and over temperatures of 55–15 °C with an average capacity of 2291 mAh at a voltage of 3.6 V.

4.2. Battery stick and module

Although individual cells can provide 3.6 V many applications required higher voltages, for example a diver thermal protection system requires from 24 to 32 V. Thus the combination of eight (8) cells in electric series provides 28.8 V and the total capacity of the system was increased by putting six (6) battery stick in parallel in an aluminum triangle. The number of batteries in series to make a stick, and the number of parallel stick can be varied to meet the specific needs of the application.

4.3. Thermal battery model

Analytical, numerical and experimental methods were used to study the temperature distributions in Li-ion battery cells during discharge. Because the discharge of the cell involves an exothermic reaction, heat is generated during use that affects the overall temperature distribution. Likewise, the ambient temperature surrounding the battery plays a role in determining the protective circuit ability to keep itself within its prescribed operating temperature range.

The volumetric heat generation is found using cell voltage, cell current, and the change in open-circuit voltage as a function of temperature. Because the change in open-circuit voltage with respect to temperature is small, the main contributor to heat generation is due to Ohmic heating, which increases as a function of time. The numerical and analytical solutions gave results that are less than 0.03% different. These results were then used to determine the temperature distribution across the radius of the battery cell, and therefore the centerline temperature. Modeling of the surface temperatures and internal temperature distribution suggested a low-Biot number, with heat transfer away from the surface due to free convection. The experimental radial temperature profiles

confirmed that the heat transfer has a low-Biot number. The temperature variation, as a function of time, was therefore modeled using a lumped capacitance model. The heat flux in 40 °C water is initially negative, reflecting the fact that the ambient temperature is larger than the temperature of the battery cell. The heat flux in 10 °C water always remained positive, but unlike the 40 °C water case, the heat flux remained relatively constant. Using the values of the heat transfer coefficient calculated from theory, it was possible to calculate the Biot number for the battery sticks, proving that the mode of heat transfer does in fact correspond to a low-Biot number situation and can be modeled using a lumped capacitance model.

During discharge in experimental conditions, the battery cells are shown to stay within their operating temperature range according to manufacturer specifications. The battery cells are therefore capable of being used for underwater applications, so long as the battery cells are not allowed to equilibrate with the outside temperature prior to use in hot water. This is important, in order to avoid thermal runaway, which may occur if the battery cells begin operation at a high initial temperature. Because of the hazards that are associated with high cell temperatures, it is suggested that the battery cells be stored in a cool environment.

4.4. Pressure collapse testing

Multiple theories were explored in this study, namely those by Levy [22], Bryan [24], Southwell [25], and Clinedinst [21]. Each theory attempted to predict the collapse pressure of a cylindrical shell, or tube, exposed to external pressurization. Experimental data were collected to validate or repudiate these theories, when applied in particular to the plastic polycarbonate tube used to protect the battery sticks in this study. The polycarbonate tubes (ν ($8.62E+07 \text{ N m}^{-2}$), E ($2.38E+09 \text{ N m}^{-2}$) and ν (0.41 mL)) used in this investigation were characterized by their length-to-thickness and diameter-to-thickness ratios. The theories used in this investigation resulted in curves that could be used for predicting collapse pressure. Each theory was shown to estimate lower values (18–39%) for the collapse pressure, when compared to experimental data. This analysis demonstrate that it is possible to compare experimental data to theoretical data, using a non-dimensional plot, with the experimental data showing the battery sticks were protected from pressure down to a depth of at least 305 m equivalent sea water.

5. General summary

This study demonstrated that Panasonic Li-ion batteries can be combined in series (sticks) to increase their available power, and also in parallel (module) to increase their capacity. The operation of the batteries cells, sticks and modules remains in their normal functional parameters over a wide range of ambient temperatures and discharge/charge rates both in air and in water. Although capacity fade has been reported for Li-ion batteries, it has not been shown to effect capacity for batteries below 4.0 V, as was the case in this study [31]. One caution is that the batteries, stick, and modules should not be stored in high ambient temperatures. The battery sticks were protected from pressure by the encasement in the polycarbonate tubes which makes them safe for operation. The battery system developed in this study is ideally suited to operate underwater gear and can be re-configured to meet the specific power demands of the application.

Disclosure

This project was funded by the Office of Naval Research and the Naval Sea Systems Command. The sponsors had no input into

the planning, conduct, or analysis of the study, or preparation or approval of the manuscript. The authors at this time have no financial conflict of interest, however a patent has been applied for by the University at Buffalo, and if licensed Drs. Pendergast and Mollendorf would receive part of the royalties by University agreement.

Acknowledgements

The authors wish to thank the Office of Naval Research and NAVSEA for their generous funding of this project. We also wish to thank Jeffery Deal, John Janis, and Chris Nebelecky, as well as the technical staff at CRESE for their technical assistance on the project.

References

- [1] E. Bardy, J.C. Mollendorf, D.R. Pendergast, *J. Phys. D: Appl. Phys.* 41 (2008) 5501–5512.
- [2] E.D. Thalmann, D.R. Pendergast, W. Mints, Establishing a Multi-center, Multi-disciplinary Program for Improving Diver Thermal Protection Hardware in Warm and Cold Water, Report to Naval Sea Coastal Systems, 2001, pp. 1–16.
- [3] J. van Zwol, *Power Elect. Tech.* July (2006) 40–45.
- [4] R. Gitzendanner, F. Puglia, C. Martin, D. Carmen, E. Jones, S. Eaves, *J. Power Sources* 136 (2004) 416–418.
- [5] P.G. Balakrishnan, R. Ramesh, T.P. Kumar, *J. Power Sources* 155 (2005) 401–414.
- [6] Energizer, Product safety datasheet. http://data.energizer.com/PDFs/lithiumion_pds.pdf, 2008 (retrieved February).
- [7] Ultralife Batteries, Material safety data sheet. <http://www.ultralifebatteries.com/documents/msdsheets/MSDS032-Li-ion.pdf>, 2008 (retrieved February).
- [8] Panasonic, Overview of lithium ion batteries. <http://www.panasonic.com/industrial/battery/oem/images/pdf/Panasonic.LiIon.Overview.pdf>, 2007 (retrieved January).
- [9] Panasonic, Notes and precautions. <http://www.panasonic.com/industrial/battery/oem/images/pdf/Panasonic.LiIon.Precautions.pdf>, 2007 (retrieved January).
- [10] C.R. Pals, *J. Electrochem. Soc.* 142 (10) (1995) 3274–3281.
- [11] W.B. Gu, C.Y. Wang, *J. Electrochem. Soc.* 147 (8) (2000) 2910–2922.
- [12] K. Onda, H. Kameyama, T. Hanamoto, K. Ito, *J. Electrochem. Soc.* 150 (3) (2003) 285–291.
- [13] L. Song, J.W. Evans, *J. Electrochem. Soc.* 147 (6) (2000) 2086–2095.
- [14] L.M. Jiji, *Heat Conduction*, Begell House, Inc., New York, NY, 2003, pp. 5–6, 35–38, 92.
- [15] F.P. Incropera, D.P. Dewitt, T.L. Bergman, A.S. Lavine, *Introduction to Heat Transfer*, John Wiley & Sons, Inc., Hoboken, NJ, 2007, pp. 8, 10, 70–74, 141, 212–218, 261, 530–535, 772–792, 840, 860.
- [16] Y. Chen, J.W. Evans, *J. Electrochem. Soc.* 143 (9) (1996) 2708–2712.
- [17] R. Haberman, *Applied Partial Differential Equations With Fourier Series and Boundary Value Problems*, Pearson Education, Inc, Upper Sadler River, NJ, 2004, pp. 347–352 (Chap. 8).
- [18] M.N. Özışik, *Heat Conduction*, John Wiley & Sons, Inc., New York, NY, 1993, pp. 215–237 (Chap. 6).
- [19] K.A. Hoffmann, S.T. Chiang, *Computational Fluid Dynamics*, Education Engineering System, Wichita, KS, 2007.
- [20] H. Maleki, S.A. Hallaj, J.R. Selman, R.B. Dinwiddie, H. Wang, *J. Electrochem. Soc.* 146 (3) (1998) 947–954.
- [21] W.O. Clinedinst, *Drilling and Prod. Pract.* (1939) 383–391.
- [22] M. Levy, *J. Mathématiques Pures Et Appliquées* (1884).
- [23] R.T. Stewart, *Trans. Am. Soc. Mech. Eng.* (1906) 730–822.
- [24] G.H. Bryan, *Proc Cambridge Phil Soc.* 1888, pp. 287–291.
- [25] R.W. Southwell, *Philos. Mag.* 2 (4) (1914) 67–77.
- [26] M.K. Yeh, S. Kyriakides, *J. Energy Res. Technol.* 108 (1) (1986) 19–26.
- [27] L. Corradi, L. Luzzi, F. Trudi, *ASME J. Appl. Mech.* 72 (4) (2005) 564–569.
- [28] H.E. Saunders, *Trans. ASME* 53 (1931) 207–218.
- [29] A.P. Carman, *Am. Phys. Soc.* (1905) 381–388.
- [30] Panasonic, Lithium ion batteries: individual data sheet. <http://www.panasonic.com/industrial/battery/oem/chem/lithion/>, 2002 (retrieved April).
- [31] R. Spotnitz, *J. Power Sources* 113 (2003) 72–80.